

Article

Studies Towards Hypoxia-Activated Prodrugs of PARP Inhibitors

Benjamin D. Dickson ^{1,2,*} , Way Wua Wong ¹, William R. Wilson ^{1,2} and Michael P. Hay ^{1,2} 

¹ Auckland Cancer Society Research Centre, School of Medical Sciences, Faculty of Medical and Health Sciences, University of Auckland, Private Bag 92019, Auckland 1010, New Zealand; w.wong@auckland.ac.nz (W.-W.W.); wr.wilson@auckland.ac.nz (W.R.W.); m.hay@auckland.ac.nz (M.P.H.)

² Maurice Wilkins Centre for Molecular Biodiscovery, University of Auckland, Symonds St, Auckland 1010, New Zealand

* Correspondence: b.dickson@auckland.ac.nz; Tel.: +64-9-923-6798

Received: 4 March 2019; Accepted: 16 April 2019; Published: 19 April 2019



Abstract: Poly(ADP-ribose)polymerase (PARP) inhibitors (PARPi) have recently been approved for the treatment of breast and ovarian tumors with defects in homologous recombination repair (HRR). Although it has been demonstrated that PARPi also sensitize HRR competent tumors to cytotoxic chemotherapies or radiotherapy, normal cell toxicity has remained an obstacle to their use in this context. Hypoxia-activated prodrugs (HAPs) provide a means to limit exposure of normal cells to active drug, thus adding a layer of tumor selectivity. We have investigated potential HAPs of model PARPi in which we attach a bio-reducible “trigger” to the amide nitrogen, thereby blocking key binding interactions. A representative example showed promise in abrogating PARPi enzymatic activity in a biochemical assay, with a ca. 160-fold higher potency of benzyl phthalazinone **4** than the corresponding model HAP **5**, but these *N*-alkylated compounds did not release the PARPi upon one-electron reduction by radiolysis. Therefore, we extended our investigation to include NU1025, a PARPi that contains a phenol distal to the core binding motif. The resulting 2-nitroimidazolyl ether provided modest abrogation of PARPi activity with a ca. seven-fold decrease in potency, but released the PARPi efficiently upon reduction. This investigation of potential prodrug approaches for PARPi has identified a useful prodrug strategy for future exploration.

Keywords: PARP inhibitor; NU1025; hypoxia-activated prodrugs; hypoxia; prodrug; anti-cancer agents; tumor targeting; radiolytic reduction

1. Introduction

Poly(ADP-ribose)polymerases (PARP) are a family of enzymes involved in the synthesis of poly(ADP-ribose) (PAR) chains from NAD⁺. Of the eighteen described members, three (PARP-1, -2, -3) have defined roles in DNA damage repair [1–4]. The role of PARP-1 is the most clearly defined and it contributes most significantly to PAR synthesis. In response to single strand breaks (SSBs) in DNA, PARP-1 binds to DNA and attaches PAR chains to nuclear proteins (PARylation) including itself (autoPARylation). The PAR chains recruit base excision repair (BER) enzymes to the SSB and ultimately lead to dissociation of PARP [1–5]. This role in DNA damage repair led to an early proposal that PARP inhibitors (PARPi) could find utility in cancer therapy [2].

PARP inhibitor cytotoxicity derives from a variety of mechanisms which have been well described elsewhere [6–11]. Briefly, catalytic inhibition of PARP stalls the BER process resulting in downstream DNA lesions when the replication forks collide with unrepaired SSB [7,12,13]. DNA lesions are also generated through the inability of inhibited PARP to dissociate from DNA, so-called “PARP trapping” [9–11]. In normal tissues, these lesions are repaired with high fidelity by homologous

recombination repair (HRR), however, in HRR incompetent cell (e.g., *BRCA1* and *BRCA2* mutants) repair occurs via low fidelity pathways, including non-homologous end joining (NHEJ), resulting in an accumulation of errors and ultimately cell death [12–14]. This combination of a genetic defect and a pharmacological treatment combining to cause cell death is a form of “synthetic lethality” and has provided the context for clinical PARPi approvals to date [14–16].

In tandem with development of potent small molecule PARPi, increased investigation of PARP biology has established involvement of the PARP family in the wider DNA damage response [3, 4]. In addition to involvement in BER, PARPs participate in HRR, canonical NHEJ (cNHEJ) and alternate end joining (alt-EJ), and have numerous interactions with nuclear proteins of unknown consequence [3,4,17,18]. Due to this widespread involvement, PARPi can sensitize cells to a variety of DNA damaging agents, and therefore combination with cytotoxic chemotherapies or radiotherapy has been proposed as an approach for treatment of HRR competent tumors [19,20]. However, studies have shown that use of PARPi in combination therapies often lead to normal tissue toxicity requiring reduction in the dose of either the PARPi or chemotherapeutic agent [21–28].

Hypoxia is a well-established feature of many solid tumors which contributes to both tumor progression and resistance to therapy [29–34]. As tumors grow, an oxygen gradient develops as its metabolic consumption outstrips the oxygen supply. Tumor vasculature lacks the organization of normal tissue vasculature which leads to tumor hypoxia, with chronic hypoxia due to oxygen diffusion limitations, and acute hypoxia caused by transient blockages or flow reversals [29,34].

We, and others, have demonstrated that hypoxia can be exploited to activate a prodrug selectively within a tumor [29,32,35]. These hypoxia-activated prodrugs (HAPs) rely on the different metabolic fates of a bio-reducible functional group (i.e., a trigger) in oxygenated versus hypoxic environments. One such trigger, the nitroaromatic group, is reduced by one-electron reductases to a nitro radical anion [29,32]. Under normoxia, this radical anion is oxidized back to the parent nitro group, whereas under hypoxia, direct fragmentation of the radical anion, or further reduction to electron-donating hydroxylamino or amino groups leads to activated species [36]. This shift in electron density can activate the drug via fragmentation of a frangible linker (e.g., evofosfamide) [37] or through activation of a reactive centre (e.g., PR-104) [38].

We considered that tumor-selective delivery of a PARPi via a HAP would increase the therapeutic index of PARPi in combination with radiotherapy or chemotherapy. To explore this proposition we started with olaparib (Lynparza) **1** as an ideal “effector” for use in a HAP as it has nanomolar potency as a PARP-1 inhibitor and recently gained first-in-class registration in an BRCA mutant advanced ovarian cancer setting as a monotherapy [15,39].

The PARPi binding mode exemplified by olaparib **1** relies on a tridentate hydrogen-bond network which mimics the natural substrate nicotinamide, Figure 1. The phthalazinone carbonyl interacts with both Ser904-OH and Gly863-NH and the amide proton interacts with Gly863-CO. Additional interactions are formed by Tyr907 and Tyr986 forming π -stacking arrangements with bound inhibitor [40].

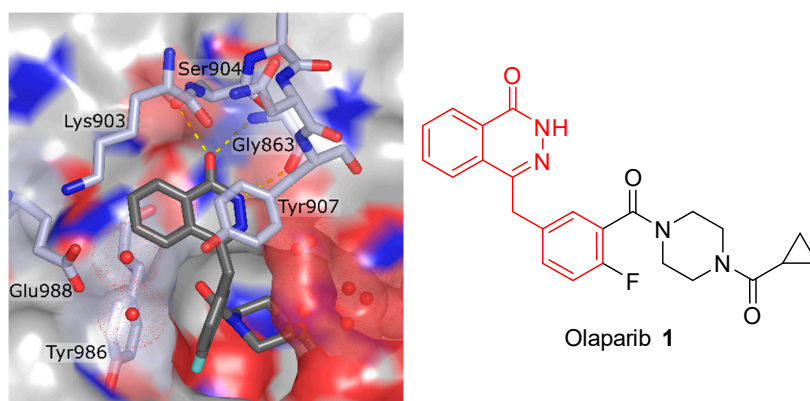


Figure 1. Olaparib **1** bound in the PARP-2 binding site (4tvj) [41].

We predicted that the addition of a 2-nitroimidazolyl trigger to the phthalazinone NH of olaparib **1** would disrupt the bonding interaction with Gly863-CO, resulting in a detrimental effect on PARP inhibition. This concept has precedence in the work of Threadgill and co-workers who installed nitroheterocyclic triggers on a series of isoquinolin-1-ones **2**, Figure 2, and demonstrated modest abrogation of PARP inhibition [42,43]. Fragmentation of 2-nitrofuryl prodrugs **3a,b** and 2-nitroimidazolyl prodrug **3c** released effectors **2a–c**, respectively, following chemical reduction (NaBH₄, Pd/C; SnCl₂; Zn/NH₄Cl) [42,43].

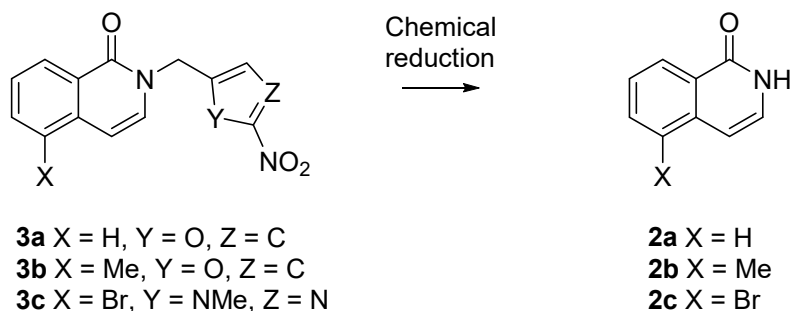


Figure 2. Reduction of nitroheterocyclic isoquinolinones **3a–c** [42,43].

To build on this initial observation and to explore the potential of this prodrug approach we prepared a series of model compounds and related 2-nitroimidazolyl derivatives based on a series of PARPi. We prepared phthalazinone **4** as a representative of the structural core of olaparib **1** and the corresponding 2-nitroimidazolyl derivative **5** as a model HAP in order to assess disruption of PARP inhibition. To assess trigger fragmentation, we prepared derivatives (**3c**, **7**, **8**, **10**, **11** and **13**, Figure 3) of model PARPi (**2a**, **2c**, **6** and **9**, Figure 3) that represent the core of literature PARPi. We also considered other possible sites of the PARPi core for placement of a trigger. The PARPi NU1025 **12**, Figure 3, contains a phenol distal to the core binding motif common to PARPi. This phenol may interact with Glu988 via a hydrogen-bond bridge with water molecules (depicted as red spheres in Figure 1) [40]. We proposed that forming a 2-nitroimidazolyl methyl ether at this phenol would hinder this interaction and could undergo fragmentation following reduction, providing an alternate prodrug strategy [44,45].

We evaluated the potency of model HAPs **5** and **13** and the associated PARPi **4** and **12** in a biochemical assay (Reaction Biology Corp, Malvern, PA) as representatives of these two approaches and investigated the stability of all model HAPs in a radiolytic reduction assay.

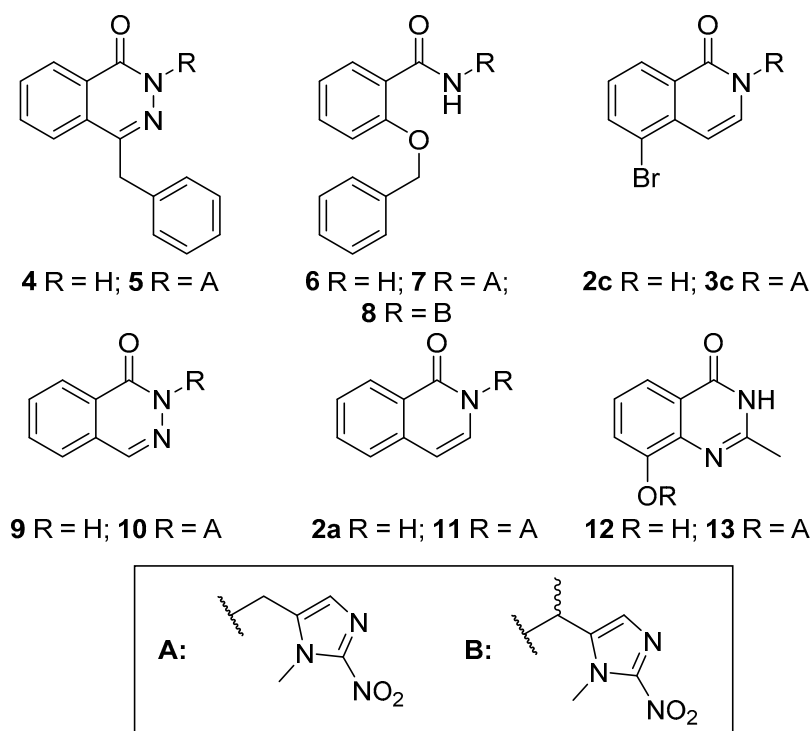


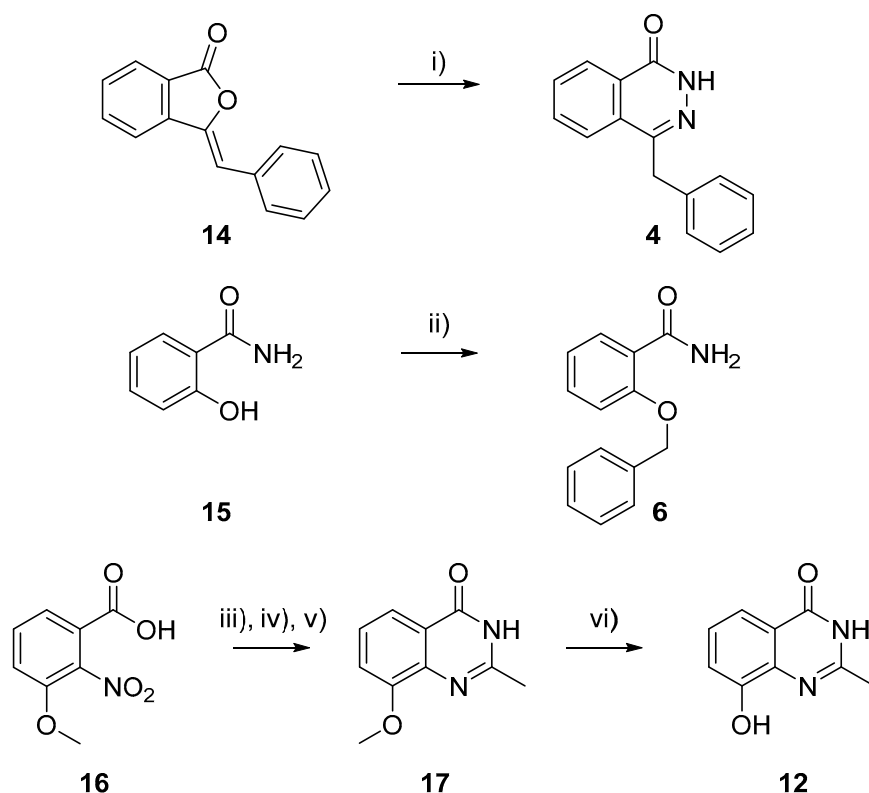
Figure 3. Poly(ADP-ribose)polymerase inhibitor (PARPi) (**2a**, **2c**, **4**, **6**, **9** and **12**) and corresponding model hypoxia-activated prodrugs (HAPs) (**3c**, **5**, **7**, **8**, **10**, **11** and **13**).

2. Results and Discussion

2.1. Synthesis

2.1.1. Synthesis of PARPi

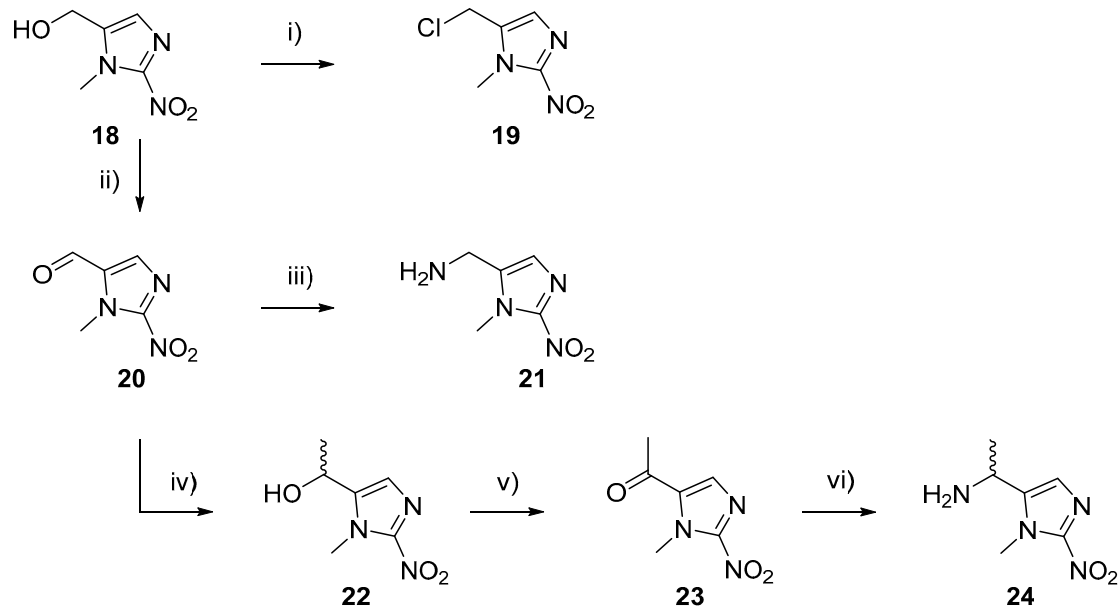
Benzyl phthalazinone **4** was prepared from isobenzofuranone **14** via addition of hydrazine hydrate, Scheme 1 [39]. Benzamide **6** was prepared by alkylation of hydroxybenzoic acid **15** in the presence of potassium iodide and potassium carbonate [46]. The remaining amide PARPi scaffolds (**2a**, **2c**, and **9**, Figure 3) were sourced commercially. The phenol containing PARPi NU1025 **12** was prepared in four steps from benzoic acid **16** as previously described by Griffin et al. [47].



Scheme 1. Synthesis of PARPi **4**, **6**, and **12**. i) NaOH, $\text{H}_2\text{NNH}_2 \cdot \text{H}_2\text{O}$, 70°C 18 h, 75%; ii) K_2CO_3 , KI, BnCl, Δ 18 h, 21%; iii) 5% Pd/C, EtOH, H_2 60 psi, 16 h, 99%; iv) CDI, DMF, 70°C , $\text{NH}_3(\text{aq})$, 16 h, 74%; v) AcCl, pyridine, THF 16 h, then 0.5 M NaOH, 1 h, 48%; and vi) BBr_3 , DCM, 30°C 72 h, 63%.

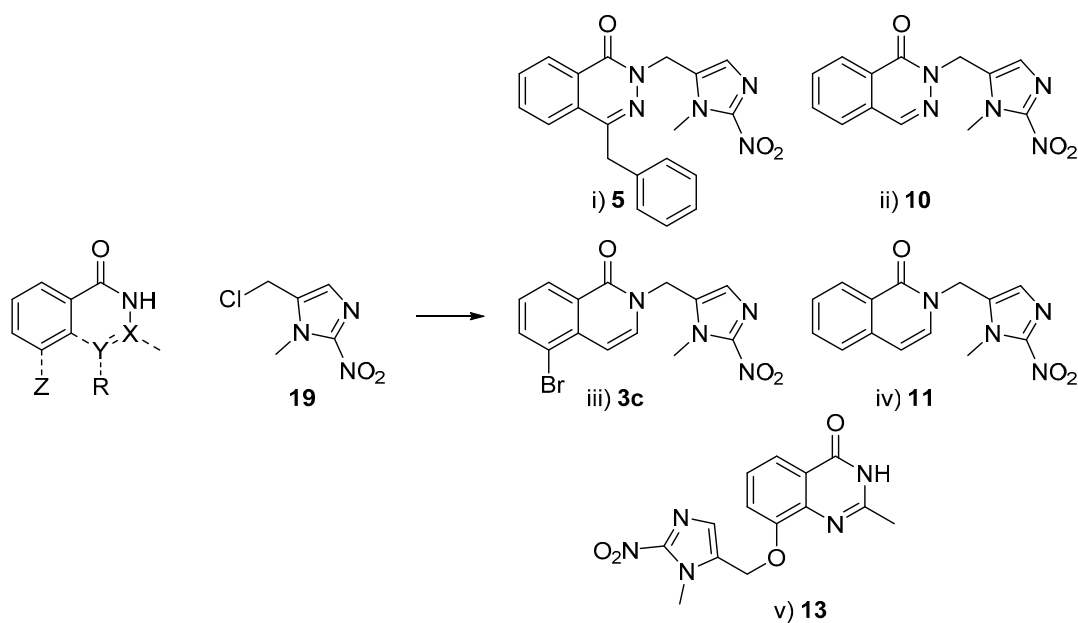
2.1.2. Synthesis of Model HAPs

The key nitroimidazole alcohol intermediate **18** was prepared following the previously described route [35,48]. Conversion to chloride **19** was achieved by mesylation of **18** and in situ chloride displacement, Scheme 2 [44]. Alcohol **18** was converted to amine **21** via reductive amination of aldehyde **20**, prepared by oxidation of **18**. Aldehyde **20** was converted to secondary alcohol **22** by addition of a methyl titanium species as described by Winn et al. [49]. Oxidation to ketone **23** was followed by reductive amination to provide secondary amine **24**. Both amines **21** and **24** were used without isolation in subsequent reactions, due to their instability.



Scheme 2. Synthesis of prodrug triggers. i) DIPEA, MsCl, 0.5 h, 91%; ii) MnO₂, Δ 18h, 76%; iii) NH₄OAc, 45 °C 2h, then NaCNBH₄, 48h, then used without purification, see Scheme 4; iv) MeMgBr, TiCl₄, −78 °C to −30 °C, −30 °C to −20 °C 3 h, 53%; v) MnO₂, Δ 18h, 81%; vi) NH₄OAc, 40 °C 1 h, then NaCNBH₄, 18 h, then used without purification, see Scheme 4.

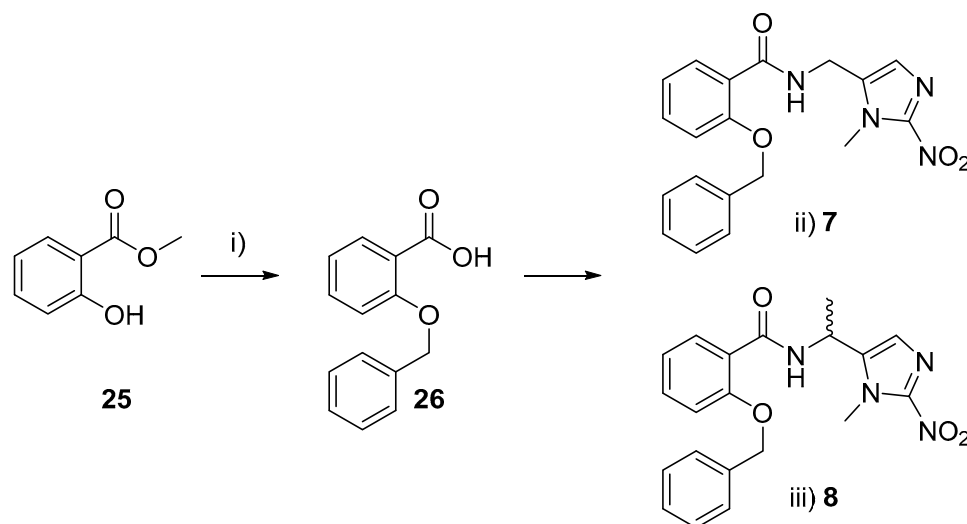
Preparation of model prodrugs **3c**, **5**, **10**, **11**, and **13** was achieved by combination of PARPi **2c**, **4**, **9**, **2a**, **12**, and **19** in the presence of a suitable base Scheme 3. LiHMDS furnished isoquinolin-1-one prodrugs **3c** and **11**, and sodium hydride was used for phthalazinone prodrugs **5** and **10**. Formation of the *N*-alkyl products was confirmed by comparison of the NCH₂ ¹³C NMR data to literature values. In *O*-alkyl products the OCH₂ resonance appears between δ 50–65, whereas the NCH₂ resonance in compounds **3c**, **5**, **10**, and **11** occurs in the range δ 30–50 as characteristic of *N*-alkylated compounds [50]. Phenoxy prodrug **13** was prepared using K₂CO₃ to deliver selective phenol alkylation.



Scheme 3. Synthesis of model HAPs **3c**, **5**, **10**, **11**, and **13**. i) NaH, 0.5 h, 50%; ii) NaH, 0.5 h, 10%; iii) LiHMDS, 2 h, NaI, 18 h, 49%; iv) LiHMDS, 18 h, 55%; v) K₂CO₃, 72 h, 47%.

In contrast alkylation of primary amide **6** did not proceed despite screening a number of bases. In an alternative approach phenol **25** was first converted to acid **26** and then the corresponding acyl chloride which was used directly to acylate amine **21** giving prodrug **7**, Scheme 4.

The fragmentation rates of 2-nitroheteroaromatic triggers are influenced by the ability of α -methylene substituents to stabilize developing positive charge in the fragmentation reaction [45]. Although an α -disubstituted trigger might be expected to provide maximal fragmentation rates these are extremely difficult to prepare [45,49]. We elected to prepare the α -substituted amide **8** to explore the influence of substitution on fragmentation rate. Formation of an acyl chloride from **26** and acylation of amine **24** yielded prodrug **8**, Scheme 4.



Scheme 4. Synthesis of primary amide PARPi prodrugs **7** and **8**. i) K_2CO_3 , BnBr, Δ 18 h, then NaOH, Δ 2 h, 82%; ii) $(COCl)_2$, 18 h, then **21**, pyridine, 0 °C–rt, 4 h, 70%; iii) $(COCl)_2$, 18 h, then **24**, pyridine, 0 °C–rt, 18 h, 29%.

2.2. Biochemical PARP-1 Inhibition

The PARP-1 inhibitory activity of the compounds was determined for the PARPi/model HAP pairs **4/5** and **12/13** in a radiometric PARP-1 inhibition assay, Table 1. Both compounds **4** and **12** were potent PARPi. Model HAP **5** provided significant (ca. 160-fold) deactivation of PARP inhibition, consistent with disruption of the key hydrogen-bonding network between the amide of PARPi **4** and PARP-1, Figure 1. In contrast, phenol prodrug **13** only showed ca. seven-fold disruption of PARP-1 inhibition, consistent with the added 2-nitroimidazolyl ether interfering with a secondary interaction, such as with Glu988, but not disrupting the key binding interactions.

Table 1. Summary of radiometric PARP-1 inhibition data.

PARPi	IC ₅₀ (μ M) ^a	Model HAP	IC ₅₀ (μ M) ^a	Ratio ^b
4	0.173 \pm 0.068	5	27.4 \pm 0.5	160 \pm 60
12	0.038 \pm 0.014	13	0.25 \pm 0.07	6.8 \pm 3.1

^a Values are mean, and errors are ranges for repeat experiments (n = 2). ^b Values are IC₅₀ ratios, and errors are root mean square of the standard error.

2.3. Radiolytic Reduction

The ability of the model HAPs to release the effectors was assessed in a radiolytic reduction assay that provides obligate one-electron reduction with well-defined stoichiometry. Radiolysis of water generates both reducing ($e^-_{(aq)}$) and oxidizing (OH^\bullet , H^\bullet) radicals but the latter can be scavenged by formate ions to generate the reducing $CO_2^{\bullet-}$ radical to give a total of 0.62 μ mol.J⁻¹ reducing

radicals [51,52]. Compounds (10 μ M) in anoxic 100 mM sodium formate/5 mM sodium phosphate buffer, pH 7.0, were irradiated (40 Gy) using a cobalt-60 source and analyzed by HPLC with in-line photodiode array absorbance and single-stage quadrupole mass spectrometry immediately after irradiation and compared with unirradiated controls. Samples were also analyzed following incubation for 5 h at 37 $^{\circ}$ C after irradiation to allow for slow fragmentation of hydroxylamine or amine intermediates to be observed. However, incubation did not alter the quantitation or identity of the species produced. Therefore, only immediate analysis results are reported. Typical results are illustrated for compounds 5, Figure 4; 3c, Figure 5; and 13, with a summary of prodrug loss and product formation in Table 2.

Table 2. Summary of radiolytic reduction results for immediate analysis following 40 Gy irradiation in anoxic formate buffer.

Model HAP	% Loss Prodrug Candidate ^a	Intermediate Species Detected ^b	% PARPi Formed ^c
3c	65.1 \pm 7.4	H (349.1/351.0 <i>m/z</i>)	n.d. ^d
5	85.3 \pm 2.1	H (362.2 <i>m/z</i>)	n.d.
7	39.2	H (353.2 <i>m/z</i>)	n.d.
8	73.9	H (367.2 <i>m/z</i>)	n.d.
10	56.3	H (272.1 <i>m/z</i>)	n.d.
11	52.3 \pm 3.6	H (271.1 <i>m/z</i>)	n.d.
13	55.0 \pm 9.1	-	39.9 \pm 7.9

^a Values are mean, and errors are ranges for duplicate samples, quantified from the absorbance chromatograms.

^b Identified by mass spectrometry as H (hydroxylamino), reported *m/z* is (M + H)⁺ for positive mode ionization.

^c Yield of PARPi as a % of initial parent compound, quantified from the absorbance chromatograms. ^d n.d., not detected.

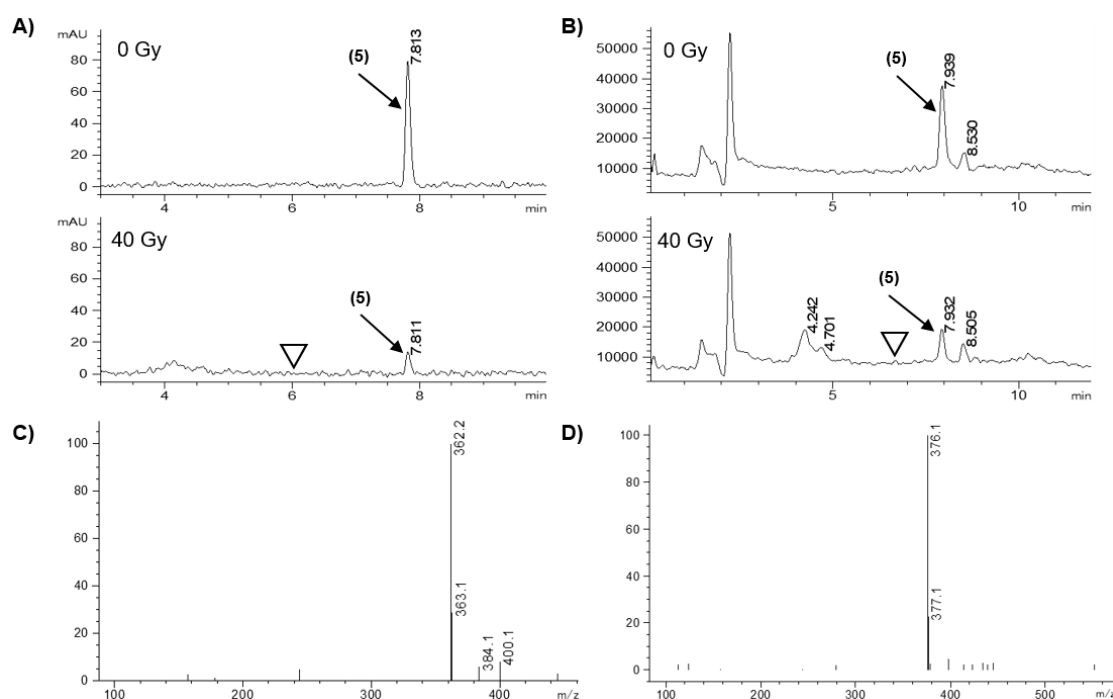


Figure 4. LC/MS analysis of the radiolytic reduction of model HAP 5. (A) Diode array chromatograms at 276 nm (bandwidth 16 nm), with 0 and 40 Gy. (B) Total ion chromatograms (positive mode, scanning *m/z* 100–600), with 0 and 40 Gy. (C) Mass spectrum of peak at retention time 4.701 min (identified as hydroxylamine). (D) Mass spectrum of peak at 7.932 min (identified as prodrug by comparison with authentic 5). ∇ Indicates the retention time of the parent PARPi 4.

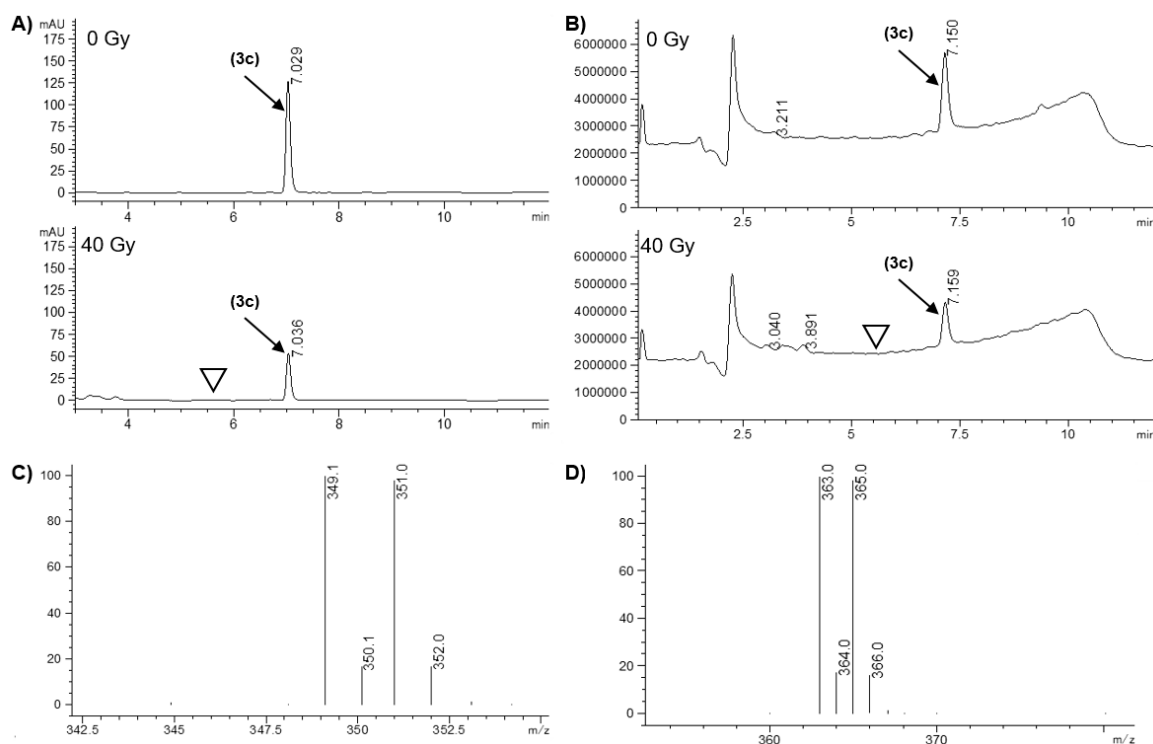


Figure 5. LC/MS analysis of the radiolytic reduction of model HAP **3c**. (A) Diode array chromatograms at 276 nm (bandwidth 16 nm), with 0 and 40 Gy. (B) Total ion chromatograms (positive mode, scanning m/z 100–600), with 0 and 40 Gy. (C) Mass spectrum of peak at 3.891 min (identified as hydroxylamine). (D) Mass spectrum of peak at 7.159 min (identified as prodrug by comparison with authentic **3c**) ∇ Indicates the retention time of the parent PARPi **2c**.

Radiolytic reduction of **5** resulted in an 85.3% decrease in diode-array signal, but we did not detect any released PARPi **4** in either the diode-array chromatogram (with comparison to authentic **4**) or the extracted ion chromatogram at the 237.1 m/z base peak, Figure 4, Table 2. Inspection of the mass spectrum revealed the hydroxylamine derivative of **5** (362.2 m/z) in the irradiated solution eluting at an earlier retention time, Figure 4. Previous studies have shown facile fragmentation of nitroheteroaromatic ethers after reduction to a hydroxylamine intermediate [45,53–55]. In this instance the stability of the hydroxylamine indicates that this system is too stable to release PARPi **4** [36,56].

We expanded our study to include analogous prodrugs based on the core scaffolds for other reported PARPi to see if the observed stability of the phthalazinone *N*-nitroimidazole framework was general [40]. We included bromoisquinolinone **3c** as it has previously been shown to fragment in a chemical reduction system [43]. We assessed all the model prodrugs in our radiolytic reduction assay, Table 2. Irradiation of amide model HAPs **3c**, **7**, **8**, **10**, and **11** resulted in loss of prodrug that was broadly consistent with the expected four-electron stoichiometry. The major products were identified as the corresponding hydroxylamines, Table 2. No evidence for the release of effectors was detected, although authentic standards were detected with high sensitivity. Solutions of the prodrugs incubated for 5 h at 37 °C post irradiation provided no evidence of effector release, suggesting slow fragmentation is unlikely. This suggests that directly-linked model HAPs of the amides, including bromoisquinolinone **3c**, Figure 5, do not readily fragment on reduction, in contrast to previous reports [42,43].

This discrepancy may be caused by the choice of reduction system. The formate radiolytic reduction system produces 4-electron reduction to the hydroxylamine species which we expected to fragment. However, we did not see evidence of 6-electron reduction to the more strongly electron-donating amino species. To address this we carried out reduction of **3c** with Zn/NH₄Cl and assessed the resulting solution by LC/MS. After one hour exposure to Zn/NH₄Cl in acetonitrile the solution was filtered and analysed by LC/MS. Comparison to a control solution allowed estimated loss of prodrug at 45% based

on the diode-array signal. At the extracted m/z 333.0 signal we detected the corresponding amino species, Figure 6A, confirmed by its mass spectrum, Figure 6B. Re-analysis of the same sample after standing for 3 h showed no change in the ion count for the amine (data not shown) and, importantly, the expected fragmentation product **2c** was not detected despite ready detection of the authentic compound, Figure 6C,D. This result strengthens our observation that this type of prodrug does not release the desired PARP inhibitor, even when reduced to the corresponding amine. We are unable to account for observation of fragmentation in previous reports.

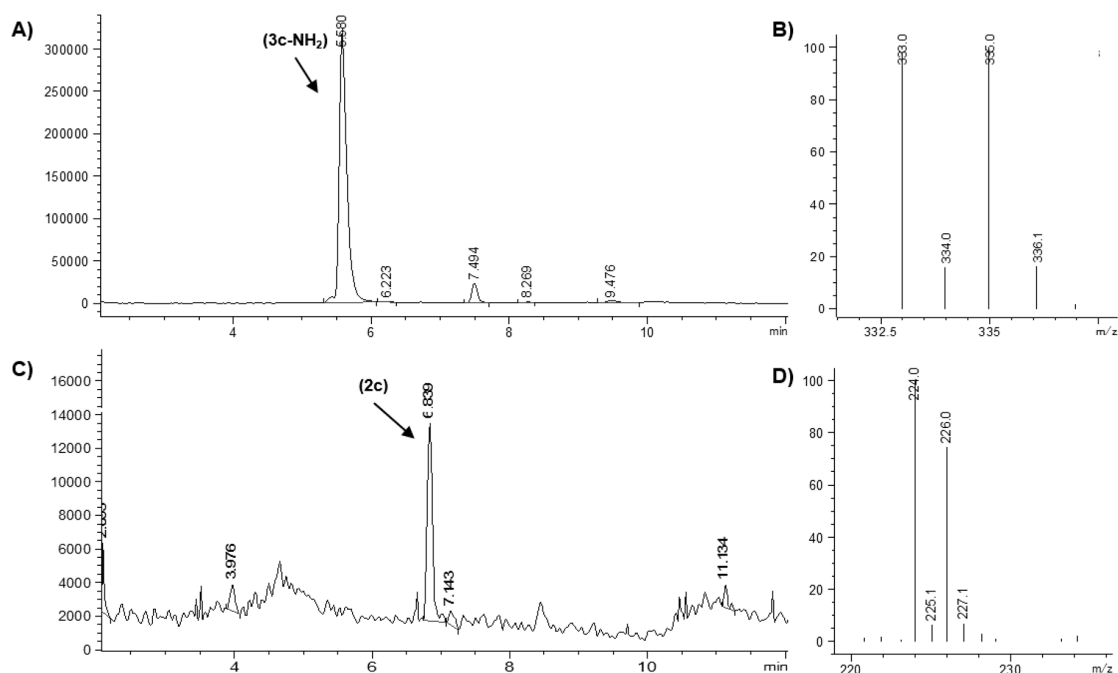


Figure 6. LC/MS analysis of the chemical reduction of model HAP **3c**. (A) Extracted ion chromatogram at m/z 333 corresponding to the Br-79 isotopologue of the amino derivative of **3c**. (B) Mass spectrum of peak at 5.580 min. (C) Extracted ion chromatogram at m/z 224 corresponding to the ^{79}Br isotopologue of **2c** from injection of a 1.8 μM solution. (D) Mass spectrum of peak at 6.839 min.

This disappointing result led us to explore a new prodrug approach. We prepared a 2-nitroimidazolyl ether linked to the phenol of NU1025 (**12**). Related prodrugs based on nitroheterocyclic ethers have been demonstrated to release effectors efficiently [44,45,49]. Reduction of the PARPi prodrug **13** did result in release of effector **12**, Table 2. Formation of **12** was detected in the diode-array chromatogram, Figure 7A, and confirmed by analysis of the mass spectrum in negative ionisation mode (**12** $[\text{M-H}]^-$ 175.1 m/z ; **13** $[\text{M-H}]^-$ 314.0 m/z , Figure 7C,D) with an efficient yield of **12** at ca. 55–60% reduction of prodrug, Table 2.

In conclusion, the *N*-alkylated nitroimidazolyl prodrug system did provide deactivation of the PARPi as intended. However, this model prodrug system does not fragment upon reduction to the corresponding hydroxylamine or amine. In contrast, the phenol prodrug **13** shows only ca. seven-fold reduction in PARP inhibition. Importantly, the 2-nitroimidazolyl ether does fragment upon reduction and this provides a lead towards identification of novel prodrugs which can combine the efficient fragmentation of the ether linker with a larger deactivation of the PARPi.

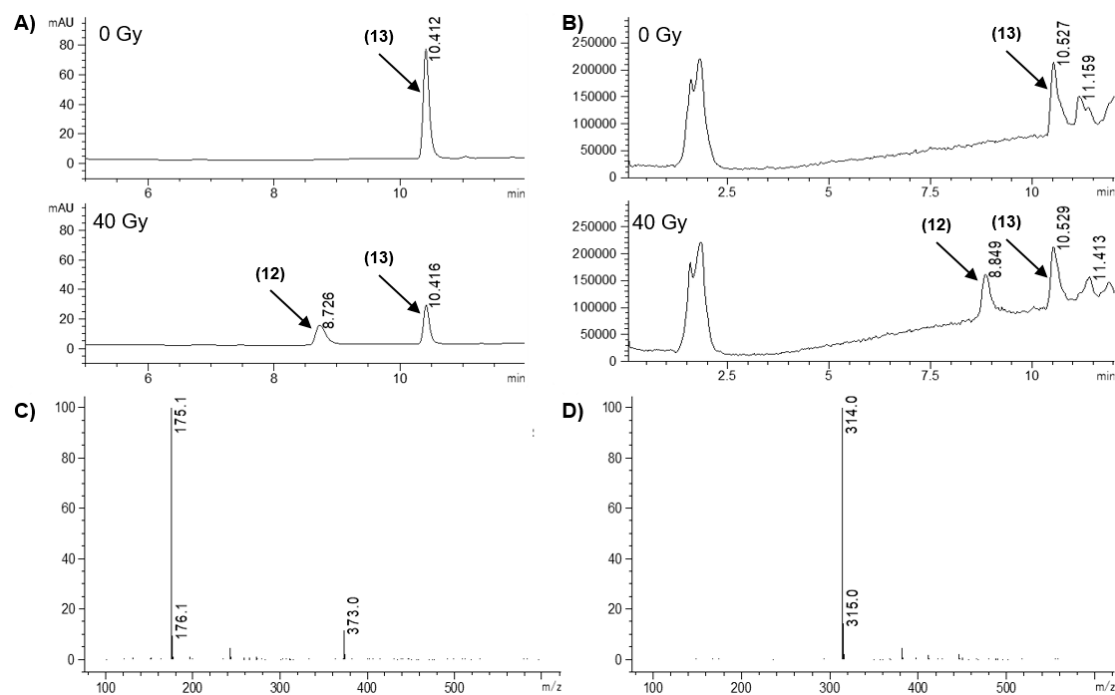


Figure 7. LC/MS analysis of the radiolytic reduction of model HAP 13. (A) Diode array chromatograms at 276 nm (bandwidth 16 nm), with 0 and 40 Gy. (B) Total ion chromatograms (negative mode, scanning m/z 100–600), with 0 and 40 Gy. (C) Mass spectrum of peak at 8.849 min (identified as effector by comparison with authentic 12). (D) Mass spectrum of peak at 10.529 min (identified as prodrug by comparison with authentic compound 13).

3. Materials and Methods

3.1. Synthesis

3.1.1. General

All non-aqueous reactions were carried out under a dry nitrogen atmosphere unless otherwise noted. DMF, DCM, and THF were purchased pre-dried and stored over molecular sieves from Acros Organics. All commercial reagents were used without purification. Flash column chromatography was carried out on a silica gel solid phase (Merck 230–400 mesh). Thin layer chromatography was carried out using Merck 60 F₂₅₄ aluminium plates pre-coated with silica. Compounds were identified using UV fluorescence and/or staining with either vanillin in ethanolic sulphuric acid (with heating), 3, 5-dinitrophenylhydrazine in ethanolic sulfuric acid (with heating), ninhydrin in ethanol/glacial acetic acid (95:5) (with heating), or iodine on silica gel. Melting points were determined on an Electrothermal 2300 melting point apparatus. High resolution mass spectra (HRMS) were measured on an Agilent Technologies 6530 Accurate-Mass Quadrupole Time-of-Flight (Q-TOF) LC/MS interfaced with an Agilent Jet Stream electrospray ionization (ESI) source allowing positive or negative ions detection. Low resolution mass spectra (LRMS) were measured on a Surveyor MSQ mass spectrometer using an atmospheric pressure chemical ionization (APCI) mode with a corona voltage of 50 V and a source temperature of 400 °C. NMR spectra data were recorded on a Bruker Avance 400 spectrometer (400 MHz, ¹H nuclei, 100 MHz, ¹³C nuclei). All chemical shift (δ) values were reported in parts per million (ppm) relative to tetramethylsilane (0.0 ppm) as an internal reference, coupling constants were reported in Hertz (Hz). Final products were analyzed by reverse-phase HPLC (Altima C18 5 μ m column, 150 mm \times 3.2 mm; Alltech Associated, Inc., Deerfield, IL) using an Agilent HP1100 equipped with a photodiode array detector. Mobile phases were gradients of 80% CH₃CN/20% H₂O (v/v) in 45 mM ammonium formate at pH 3.5 and 0.5 mL/min. Purity was determined by monitoring at 330 \pm 50 nm.

3.1.2. Procedures

5-Bromo-2-((1-methyl-2-nitro-1H-imidazol-5-yl)methyl)isoquinolin-1(2H)-one (3c). To bromoisoquinolinone **2c** (0.1 g, 0.69 mmol) in DMF (2 mL) was added a 1.0 M THF solution of LiHMDS (0.6 mL, 0.6 mmol) and the mixture was stirred for 2 h. Nitroimidazole **19** (0.08 g, 0.45 mmol) in DMF (2 mL) was added dropwise and the reaction was stirred for 2 h. NaI (0.002 g, 0.01 mmol) was added and the mixture was stirred overnight. A second addition of **19** (0.08 g, 0.45 mmol) was made and the mixture stirred a further 24 h. Water (2 mL) was added and the resulting mixture extracted with EtOAc (2 × 5 mL). The organic fractions were washed with water (5 mL), brine (5 mL) and dried over Na₂SO₄. Solvent was removed in vacuo and the crude product was purified by column chromatography (2:1, DCM, EtOAc) to yield **3c** (0.08 g, 49%) as an orange solid, mp 204–207 °C (lit. [43] mp 208–210 °C). δ_{H} (CDCl₃) 8.41 (1H, dt, $J = 7.8, 0.9$ Hz, H-6), 7.94 (1H, dd, $J = 7.7, 1.2$ Hz, H-8), 7.39 (1H, t, $J = 7.9$ Hz, H-7), 7.23 (1H, s, H-4'), 7.14 (1H, d, $J = 7.7$ Hz, H-3), 6.94 (1H, dd, $J = 7.7, 0.6$ Hz, H-4), 5.30 (2H, s, CH₂), 4.06 (3H, s, CH₃). δ_{C} ((CD₃)₂SO) 160.3 (C = O), 145.8 (C), 136.4 (CH), 135.8 (C), 134.2 (C), 133.9 (CH), 128.0 (CH), 127.9 (CH), 127.3 (CH), 126.9 (CH), 120.0 (C), 104.0 (CH), 41.3 (CH₂), 34.3 (CH₃). HRMS calcd for C₁₄H₁₂⁷⁹BrN₄O₃ (M + H) m/z 363.0093, found 363.0087; for C₁₄H₁₂⁸¹BrN₄O₃ (M + H) m/z 365.0073, found 365.0071. LRMS m/z 363.0 (100%, M⁷⁹ + H), 365.0 (95%, M⁸¹ + H). HPLC purity: 95.5% (effector **2c**: not detected).

4-Benzylphthalazin-1(2H)-one (4). To a stirred suspension of benzaldehyde **14** (10 g, 45 mmol) in water (60 mL) was added aqueous NaOH (13 M, 15 mL) and the mixture was heated to 70 °C. Hydrazine hydrate (31 mL, 630 mmol) was added and the mixture stirred for 18 h. The reaction was cooled to room temperature and acidified with 8 M aqueous HCl to pH 4. After 10 min the resulting suspension was filtered and washed with water (2 × 50 mL) and diethyl ether (3 × 50 mL) to yield **4** (8.0 g, 75%) as a white solid, mp 198–200 °C (lit. [57] mp 200–201 °C). δ_{H} (CDCl₃) 9.95 (1H, br s, NH), 8.47–8.43 (1H, m, H-8), 7.79–7.71 (3H, m, H-5, H-6, H-7), 7.33–7.00 (5H, m, Ar-H), 4.30 (2H, s, CH₂Ph). δ_{C} (CDCl₃) 161.1 (C = O), 146.5 (C), 137.8 (C), 133.6 (CH), 131.5 (CH), 130.0 (C), 128.9 (2 × CH), 128.7 (2 × CH), 128.5 (C), 127.2 (CH), 127.0 (CH), 125.6 (CH), 39.1 (CH₂). LRMS m/z 237.2 (100%, M + H). HPLC purity: 99.2%. These data are in good agreement with literature values [57].

4-Benzyl-2-((1-methyl-2-nitro-1H-imidazol-5-yl)methyl)phthalazin-1(2H)-one (5). To phthalazinone **4** (0.33 g, 1.40 mmol) in DMF (2 mL) was added NaH (60% dispersion in mineral oil) (0.084 g, 2.10 mmol) and the resulting solution stirred for 30 min at room temperature. Nitroimidazole **19** (0.34 g, 1.94 mmol) was added and the solution was stirred for 30 min, then quenched on ice. The mixture was extracted with EtOAc (10 mL), washed with water (3 × 10 mL), dried over MgSO₄ and solvent removed in vacuo. The crude product which was purified by column chromatography (1:1 X4, EtOAc) to yield **5** (0.10 g, 50%) as a yellow solid, mp 180–182 °C. δ_{H} ((CD₃)₂SO) 8.31 (1H, dd, $J = 7.6, 1.4$ Hz, H-8), 8.00 (1H, dd, $J = 8.2, 1.0$ Hz, H-5), 7.91–7.83 (2H, m, H-6, H-7), 7.30–7.24 (4H, m, Ar-H), 7.21–7.17 (2H, m, H-4', Ar-H), 5.45 (2H, s, CH₂N), 4.31 (2H, s, CH₂Ph), 3.93 (3H, s, CH₃). δ_{C} ((CD₃)₂SO) 158.0 (C = O), 145.9 (C), 145.6 (C), 137.7 (C), 134.0 (C), 133.6 (CH), 132.0 (CH), 128.7 (2 × CH), 128.4 (2 × CH), 128.36 (CH), 128.36 (CH), 127.3 (C), 126.5 (2 × CH), 125.8 (CH), 43.4 (CH₂), 37.5 (CH₂) 34.4 (CH₃). HRMS calcd for C₂₀H₁₈N₅O₃ (M + H) m/z 376.1404, found 376.1412. LRMS m/z 376.2 (100%, M + H). HPLC purity: 96.1% (effector **4**: 0.3%).

2-(Benzylloxy)benzamide (6). To amide **15** (0.80 g, 5.83 mmol), K₂CO₃ (0.97 g, 7.02 mmol) and KI (1.17 g, 7.02 mmol) in acetone (30 mL) was added benzyl chloride (0.81 mL, 7.02 mmol), and the reaction stirred at reflux for 18 h. The solution was cooled and filtered and solvent removed in vacuo. The crude product was recrystallised from acetone to yield **6** (0.28 g, 21%) as a cream solid, mp 112–114 °C (lit. [58] mp 115–116 °C). δ_{H} (CDCl₃) 8.25 (1H, dd, $J = 7.8, 1.8$ Hz, H-6), 7.73 (1H, br s, NH), 7.50–7.37 (6H, m, Ar-H), 7.13–7.06 (2H, m, Ar-H), 5.81 (1H, br s, NH), 5.20 (2H, s, CH₂). δ_{C} (CDCl₃) 167.1 (C = O), 157.3 (C), 136.8 (C), 133.6 (CH), 132.9 (CH), 129.2 (2 × CH), 128.9 (CH), 128.1 (2 × CH), 121.7 (CH), 121.3 (C), 112.9 (CH), 71.5 (CH₂). LRMS m/z 228.2 (100%, M + H). HPLC purity: 100%. These data are in good agreement with literature values [59].

2-(Benzylloxy)-N-((1-methyl-2-nitro-1H-imidazol-5-yl)methyl)benzamide (7). (1-Methyl-2-nitro-1H-imidazol-5-yl)methanamine (**21**). To aldehyde **20** (0.60 g, 3.87 mmol) in MeOH (16 mL)

was added ammonium acetate (5.96 g, 77.4 mmol) and the mixture was stirred at 45 °C for 2 h. NaCNBH₄ (0.17 g, 2.37 mmol) was added and the mixture stirred for 48 h, acidified to pH 1 with 6 M aqueous HCl and solvent removed in vacuo. The aqueous residue was filtered and the filtrate basified to pH 14 with 6 M aqueous KOH. The aqueous was extracted with DCM (3 × 50 mL), then saturated with NaCl and further extracted with DCM (3 × 50 mL). The combined organic fractions were concentrated and filtered through a plug of silica (9:1, DCM, MeOH) to give a crude residue **21** (0.15 g) which was used without further purification. δ_{H} ((CD₃)₂SO) 7.07 (1H, s, H-4), 3.90 (3H, s, CH₃), 3.77 (2H, s, CH₂), 3.17 (2H, br s, NH₂).

To benzoic acid **26** (0.16 g, 0.704 mmol) in DCM (3 mL) was added oxalyl chloride (0.30 mL, 3.54 mmol) and the mixture was stirred overnight at room temperature. Solvent was removed in vacuo. The crude residue was taken up in DCM (2 mL) and added to a solution of amine **21** (0.10 g, 0.64 mmol) in pyridine (2 mL) at 0 °C. The mixture was allowed to come to room temperature and stirred for 4 h. Solvent was removed in vacuo and the crude residue was purified by column chromatography (2:1, EtOAc, X4) to yield **7** (0.16 g, 70%) as yellow solid, mp 120–122 °C. δ_{H} ((CD₃)₂SO) 8.62 (1H, t, *J* = 5.5 Hz, NH), 7.67 (1H, dd, *J* = 7.6, 1.7 Hz, H-6), 7.49–7.43 (1H, m, H-4), 7.42–7.38 (2H, m, Ar-H), 7.33–7.26 (3H, m, Ar-H), 7.22 (1H, d, *J* = 7.8 Hz, H-3), 7.07–7.02 (2H, m, H-5, H-4'), 5.19 (2H, s, OCH₂), 4.55 (2H, d, *J* = 5.6 Hz, NCH₂), 3.75 (3H, s, NCH₃). δ_{C} ((CD₃)₂SO) 165.5 (C = O), 155.8 (C), 145.4 (C), 136.4 (C), 136.0 (C), 132.1 (CH), 130.0 (CH), 128.3 (2 × CH), 127.9 (CH), 127.6 (2 × CH), 127.2 (CH), 123.8 (C), 120.7 (CH), 113.3 (CH), 70.0 (CH₂), 33.9 (CH₃), 33.1 (CH₂). HRMS calcd for C₁₉H₁₉N₄O₄ (M + H) *m/z* 367.1401, found 367.1407. LRMS *m/z* 367.2 (100%, M + H). HPLC purity: 99.3% (effector **6**: not detected).

2-(Benzyloxy)-N-(1-(1-methyl-2-nitro-1H-imidazol-5-yl)ethyl)benzamide (8). 1-(1-Methyl-2-nitro-1H-imidazol-5-yl)ethan-1-amine (**24**). To ketone **23** (0.20 g, 1.2 mmol) in MeOH (4 mL) was added ammonium acetate (1.8 g, 23.6 mmol) and the resulting solution was stirred at 40 °C for 1 h. Activated 4 Å molecular sieves were added and the mixture was stirred a further 1 h. The mixture was cooled to 0 °C and NaCNBH₄ (0.05 g, 0.84 mmol) added, then the mixture was warmed to room temperature and stirred overnight. Solvent was removed in vacuo and the resulting residue filtered through a plug of silica (9:1, DCM, MeOH) to give a crude residue **24** (0.04 g) which was used without further purification. δ_{H} ((CD₃)₂SO) 7.10 (1H, s, H-4), 4.05 (1H, q, *J* = 6.7 Hz, CH), 3.94 (3H, s, NCH₃), 1.38 (3H, d, *J* = 6.7 Hz, CH₃).

To benzoic acid **26** (0.06 g, 0.26 mmol) in DCM (1 mL) added oxalyl chloride (0.11 mL, 3.54 mmol) and the mixture was stirred overnight at room temperature. Solvent was removed in vacuo. The crude residue was taken up in DCM (1 mL) and added to a solution of amine **24** (0.04 g, 0.24 mmol) in pyridine (0.5 mL) at 0 °C. The mixture was allowed to come to room temperature and stirred overnight. Solvent was removed in vacuo and the crude residue was purified by column chromatography (2:1, X4, EtOAc) to yield **8** (0.026 g, 29%) as a white solid, mp 151–153 °C. δ_{H} (CDCl₃) 8.22 (1H, dd, *J* = 7.8, 1.8 Hz, H-6), 8.08 (1H, d, *J* = 8.2 Hz, NH), 7.54–7.50 (1H, m, H-4), 7.43–7.28 (5H, m, Ar-H), 7.15 (1H, td, *J* = 7.2, 1.0 Hz, H-5), 7.10 (1H, d, *J* = 8.3 Hz, H-3), 6.81 (1H, d, *J* = 0.6 Hz, H-4'), 5.36 (1H, p, *J* = 8.0 Hz, CH), 5.08 (2H, ddd, *J* = 10.8, 9.8, 9.8 Hz, OCH₂), 3.84 (3H, s, NCH₃), 1.44 (3H, d, *J* = 6.9 Hz, CH₃). δ_{C} (CDCl₃) 164.5 (C = O), 157.1 (C), 139.3 (C), 135.0 (C), 133.7 (CH), 132.7 (CH), 129.5 (CH), 129.2 (2 × CH), 128.4 (2 × CH), 126.0 (CH), 122.2 (CH), 120.8 (C), 112.5 (CH), 71.9 (CH₂), 39.8 (CH), 34.4 (CH₃), 19.5 (CH₃); C-NO₂ was not observed. HRMS calcd for C₂₀H₂₁N₄O₄ (M + H) *m/z* 381.1571, found 381.1568. LRMS *m/z* 381.2 (100%, M + H). HPLC purity: 99.8% (effector **6**: not detected).

2-((1-Methyl-2-nitro-1H-imidazol-5-yl)methyl)phthalazin-1(2H)-one (10). To phthalazinone **9** (0.205 g, 1.40 mmol) in DMF (2 mL) was added NaH (60% dispersion in mineral oil) (0.084 g, 2.10 mmol) and the resulting solution stirred for 30 min at room temperature. Nitroimidazole **19** (0.27 g, 1.54 mmol) was added and the solution was stirred for 30 min, then quenched on ice. The resulting suspension was filtered, the collected solid washed with water (5 mL), X4 (5 mL) and dried in vacuo to yield **10** (0.04 g, 10%) as a yellow solid, mp 207–209 °C. δ_{H} ((CD₃)₂SO) 8.49 (1H, s, H-4), 8.29 (1H, dd, *J* = 7.84, 0.7 Hz, H-8), 7.98 (2H, d, *J* = 3.7 Hz, H-7, H-6), 7.93–7.87 (1H, m, H-5), 7.19 (1H, s, H-4'), 5.47 (2H, s, CH₂), 4.00 (3H, s, CH₃). δ_{C} ((CD₃)₂SO) 158.4 (C = O), 145.6 (C), 138.9 (C), 134.1 (C), 133.9 (C), 132.4

(CH), 129.3 (C), 128.4 (CH), 127.1 (CH), 127.9 (C), 125.9 (CH), 43.6 (CH₂), 34.4 (CH₃). HRMS calcd for C₁₃H₁₂N₅O₃ (M + H) *m/z* 286.0935, found 286.0941. LRMS *m/z* 286.1 (100%, M + H). HPLC purity: 94.4% (effector **10**: 0.1%).

2-((1-Methyl-2-nitro-1H-imidazol-5-yl)methyl)isoquinolin-1(2H)-one (11). To isoquinolinone **2a** (0.10 g, 0.69 mmol) in DMF (2 mL) was added a 1.0 M THF solution of LiHMDS (0.90 mL, 0.90 mmol) and the mixture was stirred for 2 h. Nitroimidazole **19** (0.12 g, 0.69 mmol) in DMF (2 mL) was added dropwise and the reaction was stirred overnight. Water (2 mL) was added and the resulting mixture extracted with EtOAc (2 × 5 mL). The organic fractions were washed with water (5 mL), brine (5 mL) and dried over Na₂SO₄. Solvent was removed in vacuo and the crude product was purified by column chromatography (2:1, DCM, EtOAc) to yield **11** (0.11 g, 55%) as a yellow solid, mp 207–210 °C. δ_H ((CD₃)₂SO) 8.25 (1H, dt, *J* = 8.1, 0.6 Hz, H-8), 7.74 (1H, ddd, *J* = 9.2, 7.0, 1.3 Hz, H-6), 7.68 (1H, dd, *J* = 7.9, 0.7 Hz, H-7) 7.55 (2H, d, *J* = 7.6 Hz, H-5, H-3), 7.16 (1H, s, H-4'), 6.71 (1H, d, *J* = 7.4 Hz, H-4), 5.33 (2H, s, CH₂), 3.99 (3H, s, CH₃). δ_C ((CD₃)₂SO) 161.0 (C = O), 145.7 (C), 136.9 (C), 134.6 (C), 132.7 (CH), 132.0 (CH), 127.8 (CH), 127.1 (CH), 127.0 (CH), 126.3 (CH), 125.2 (C), 106.0 (CH), 40.9 (CH₂), 34.3 (CH₃). HRMS calcd for C₁₄H₁₃N₄O₃ (M + H) *m/z* 285.0982, found 285.0978. LRMS 2 *m/z* 85.1 (100%, M + H). HPLC purity: 96.7% (effector **2a**: not detected).

8-Hydroxy-2-methylquinazolin-4(3H)-one (12). To a stirred solution of quinazolinone **17** (400 mg, 2.10 mmol) in dry DCM (10 mL) was added a 1.0 M DCM solution of BBr₃ (4.8 mL, 4.8 mmol) and the mixture stirred at 30 °C for 72 h. Solvent was removed in vacuo, the residue cooled to 5 °C and aqueous NaOH (2.5 M, 30 mL) was added. The mixture was stirred at 20 °C for 15 min, filtered and the pH of the filtrate adjusted to 5 with aqueous HCl (6 M). The mixture was chilled at 5 °C for 1 h. The resulting precipitate was purified by column chromatography (1:1–1:0, EtOAc, X4) to yield **12** (0.23 g, 63%) as a tan powder, mp 261–263 °C (lit. [47] mp 253–258 °C). δ_H ((CD₃)₂SO) 12.14 (1H, br s, NH), 9.36 (1H, s, OH), 7.49 (1H, dd, *J* = 7.9, 1.4 Hz, H-5), 7.25 (1H, t, *J* = 7.9 Hz, H-6), 7.14 (1H, dd, *J* = 7.8, 1.4 Hz, H-7), 2.37 (3H, s, 2-CH₃). δ_C ((CD₃)₂SO) 162.2 (C = O), 153.0 (C), 152.7 (C), 138.4 (C), 126.7 (CH), 121.9 (C), 118.6 (CH), 115.9 (CH), 21.9 (CH₃). LRMS *m/z* 177.2 (100%, M + H). These data are in good agreement with literature values [47,60].

2-Methyl-8-((1-methyl-2-nitro-1H-imidazol-5-yl)methoxy)quinazolin-4(3H)-one (13). To phenol **12** (0.069 g, 0.39 mmol) in DMF (2 mL) was added K₂CO₃ (0.16 g, 1.16 mmol) followed by nitroimidazole **19** (0.069 g, 0.57 mmol). The mixture was stirred for 72 h, diluted with water and collected by filtration. The crude compound was purified by column chromatography (40:1, DCM, MeOH) to yield **13** (0.057 g, 47%) as a white solid, mp 253–256 °C. δ_H ((CD₃)₂SO) 12.24 (1H, br s, NH), 7.72 (1H, dd, *J* = 8.0, 1.1 Hz, H-5), 7.54 (1H, dd, *J* = 8.0, 1.1 Hz, H-7), 7.39 (1H, t, *J* = 8.0 Hz, H-6), 7.39 (1H, s, H-4'), 5.38 (2H, s, CH₂), 4.06 (3H, s, NCH₃), 2.34 (3H, s, CH₃). δ_C ((CD₃)₂SO) 161.5 (C = O), 153.4 (C), 152.1 (C), 140.5 (C), 133.5 (C), 128.6 (CH), 125.9 (CH), 122.0 (C), 119.2 (CH), 118.7 (CH), 61.0 (CH₂), 34.3 (CH₃), 21.6 (CH₃); C-NO₂ was not observed. HRMS calcd for C₁₄H₁₄N₅O₄ (M + H) *m/z* 316.1040, found 316.1039. LRMS *m/z* 316.1 (100%, M + H). HPLC purity: 95.6% (effector **12**: 0.4%).

8-Methoxy-2-methylquinazolin-4(3H)-one (17). A mixture of acid **16** (8.37 g, 42.5 mmol) and Pd/C (5%, 0.10 g) in EtOH (100 mL) was stirred under H₂ (60 psi) for 16 h. The mixture was filtered through diatomaceous earth, the pad washed with EtOH (50 mL) and solvent removed in vacuo to give 2-amino-3-methoxybenzoic acid (7.05 g, 99%) as a tan powder which was used directly. CDI (6.70 g, 41.3 mmol) was added to a stirred solution of 2-amino-3-methoxybenzoic acid (7.05 g, 42.2 mmol) in dry DMF (100 mL) at 70 °C and the mixture stirred for 10 min. A solution of aqueous NH₃ (108 mL, 1.05 mol) was added slowly and the mixture was stirred at 70 °C for 16 h. The mixture was cooled to 20 °C, diluted with EtOAc (300 mL), washed with water (3 × 100 mL), brine (100 mL), dried (MgSO₄) and solvent removed in vacuo to give crude 2-amino-3-methoxybenzamide (5.21 g, 74%) as a tan solid which was used directly. Acetyl chloride (1.43 mL, 20.2 mmol) in dry THF (2 mL) was added dropwise to a stirred solution of 2-amino-3-methoxybenzamide (1.66 g, 10.0 mmol) and pyridine (1.06 mL, 13.0 mmol) in dry THF (50 mL) at 20 °C and the resulting mixture stirred for 16 h. Solvent was removed in vacuo, the residue dissolved in aqueous NaOH (0.5 M, 25 mL) and stirred

for 1 h. The solution was carefully neutralized with aqueous HCl (0.5 M) and stirred at 5 °C for 1 h. The precipitate was filtered and recrystallized from MeOH/water to yield **17** (0.91 g, 48%) as a white solid, mp 263–266 °C (lit. [61] mp 262–263 °C). δ_{H} ((CD₃)₂SO) 10.79 (1H, br s, NH), 7.61 (1H, dd, $J = 7.8$, 1.4 Hz, H-5), 7.36 (1H, t, $J = 7.9$ Hz, H-6), 7.30 (1H, dd, $J = 8.0$, 1.4 Hz, H-7), 3.87 (3H, s, OCH₃), 2.34 (3H, s, CH₃). δ_{C} ((CD₃)₂SO) 161.7 (C = O), 154.0 (C), 152.9 (C), 139.4 (C), 126.0 (CH), 121.6 (C), 116.7 (CH), 114.7 (CH), 55.8 (CH₃), 21.5 (CH₃). LRMS m/z 191.1 (100%, M + H). These data are in good agreement with literature values [60,61].

5-(Chloromethyl)-1-methyl-2-nitro-1H-imidazole (19). To a solution of alcohol **18** (0.50 g, 3.2 mmol) in THF (10 mL) at 0 °C was added diisopropylethylamine (0.67 mL, 3.8 mmol) and methanesulfonyl chloride (0.3 mL, 0.38 mmol) and the mixture was stirred for 30 min. EtOAc (20 mL) was added and the solution washed with 1M aqueous HCl (20 mL), dried over MgSO₄ and solvent removed in vacuo. The crude material was purified by column chromatography (2:1, X4, EtOAc) to yield **19** (0.51 g, 91%) as a yellow solid, mp 99–100 °C (lit. [43] mp 94–96 °C). δ_{H} (CDCl₃) 7.19 (1H, s, 4-H), 4.63 (2H, s, CH₂), 4.08 (3H, s, CH₃). δ_{C} (CDCl₃) 146.4 (C-NO₂), 132.9 (C), 128.6 (CH), 34.3 (CH₃), 33.9 (CH₂). LRMS m/z 176.1 (100%, M³⁵ + H), 178.1 (36%, M³⁷ + H). These data are in good agreement with literature values [43].

1-Methyl-2-nitro-1H-imidazole-5-carbaldehyde (20). To alcohol **18** (1.0 g, 6.36 mmol) in chloroform (70 mL) was added MnO₂ (2.76 g, 31.8 mmol) and the mixture was heated to reflux overnight. After cooling, the resulting slurry was filtered through diatomaceous earth and solvent removed in vacuo to yield **19** (1.5 g, 76%) as a pale yellow solid, mp 112–114 °C (lit. [62] mp 114–115 °C). δ_{H} (CDCl₃) 9.93 (1H, s, CHO), 7.81 (1H, s, H-4), 4.36 (3H, s, CH₃). δ_{C} (CDCl₃) 180.4 (C = O), 148.3 (C-NO₂), 139.4 (CH), 132.4 (CH), 35.6 (CH₃). LRMS 188.1 (100%, M + CH₃OH). These data are in good agreement with literature values [35].

1-(1-Methyl-2-nitro-1H-imidazol-5-yl)ethan-1-ol (22). A 3 M solution of MeMgBr in Et₂O (0.32 mL, 0.97 mmol) was added to a solution of TiCl₄ (0.11 mL, 0.97 mmol) in DCM (4 mL) at –78 °C. The mixture was allowed to warm to –30 °C and added to a solution of aldehyde **20** (0.15 g, 0.97 mmol) in DCM (4 mL) at –30 °C. This mixture was maintained at –30 to –20 °C for 3 h, then quenched by addition of saturated aqueous NH₄Cl (5 mL). The aqueous fraction was extracted with DCM (3 × 10 mL) and solvent removed in vacuo. The crude mixture was purified by column chromatography (50:1, DCM, MeOH) to yield **22** (0.09 g, 53%) as an orange solid, mp 101–103 °C. δ_{H} (Acetone-*d*₆) 7.06 (1H, s, H-4), 5.05–4.94 (1H, m, CH), 4.59 (1H, br s, OH), 4.08 (3H, s, NCH₃), 1.61 (3H, d, $J = 6.6$ Hz, CH₃). δ_{C} (Acetone-*d*₆) 147.3 (C-NO₂), 141.6 (C), 124.7 (CH), 60.3 (CH), 33.9 (CH₃), 21.1 (CH₃). LRMS m/z 172.2 (100%, M + H). These data are in good agreement with literature values [49].

1-(1-Methyl-2-nitro-1H-imidazol-5-yl)ethan-1-one (23). To a solution of alcohol **22** (0.06 g, 0.35 mmol) in CHCl₃ (10 mL) was added MnO₂ (0.20 g, 2.3 mmol) and the resulting solution was stirred at reflux overnight. The resulting slurry was filtered through diatomaceous earth and solvent was removed in vacuo to yield **23** (0.048 g, 81%) as a yellow solid, mp 71–72 °C (lit. [62] mp 81–83 °C). δ_{H} (CDCl₃) 7.77 (1H, s, H-4), 4.32 (3H, s, NCH₃), 2.59 (3H, s, CH₃). δ_{C} (CDCl₃) 189.2 (C = O), 148.2 (C-NO₂), 135.7 (CH), 132.3 (C), 35.8 (CH₃), 28.6 (CH₃). HRMS calcd for C₆H₇N₃O₃ (M + H) m/z 170.0560, found 170.0556. LRMS m/z 170.1 (100%, M + H).

2-(Benzyloxy)benzoic acid (26). To ester **25** (1.60 mL, 12.04 mmol) in MeCN (50 mL) was added K₂CO₃ (3.30 g, 24.08 mmol) followed by benzyl bromide (1.50 mL, 12.88 mmol) and the resulting mixture was stirred at reflux overnight. After cooling the reaction was diluted with water (25 mL) and the aqueous fraction extracted with DCM (3 × 20 mL). The combined organic extracts were washed with water (25 mL), dried over Na₂SO₄ and solvent removed in vacuo. The crude residue was dissolved in 1,4-dioxane (50 mL) and aqueous NaOH (1.5 M, 12 mL) was added. The solution was stirred at reflux for 2 h, cooled to room temperature and the organic residues removed in vacuo. The remaining solution was acidified with 1M aqueous HCl, extracted with EtOAc (3 × 25 mL), the organic extracts dried over Na₂SO₄ and solvent removed in vacuo to yield **26** (2.4 g, 82%) as a colourless solid, mp 70–71 °C (lit. [63] mp 73–75 °C). δ_{H} (CDCl₃) 10.72 (1H, br s, OH), 8.21 (1H, dd, $J = 7.8$, 1.8 Hz, H-6),

7.56 (1H, ddd, $J = 9.2, 7.4, 1.8$ Hz, H-4), 7.46–7.38 (5H, m, Ar-H), 7.18–7.11 (2H, m, H-5, H-3) 5.30 (2H, s, CH₂). δ_C (CDCl₃) 165.6 (C = O), 157.6 (C), 135.2 (CH), 134.5 (C), 134.0 (CH), 129.34 (CH), 129.32 (2 × CH), 128.1 (2 × CH), 122.6 (CH), 118.2 (C), 113.3 (CH), 72.4 (CH₂). LRMS m/z 229.2 (100%, M + H). These data are in good agreement with literature values [64].

3.2. Assays

3.2.1. Radiolytic Reduction

DMSO stock solutions (10 mM) were transferred to a Pd/C catalyzed anaerobic chamber with an atmosphere of 5% H₂, 5% CO₂, 90% N₂ (Shellab Bacatron, Sheldon Manufacturing Inc. Cornelius, OR), and diluted to make 10 μ M solutions in 100 mM sodium formate/5 mM sodium phosphate, pH 7.0, using buffer that had been equilibrated in the chamber for ≥ 3 days to ensure deoxygenation. Aliquots (1 mL) were then transferred to HPLC vials, sealed, removed from the chamber and irradiated using an Eldorado 78 teletherapy cobalt-60 unit. The dose rate was ~ 3 Gy/min, with exact values determined by Fricke dosimetry [65]. Samples were analyzed immediately by LC/MS, or after incubating for 5 h at 37 °C.

3.2.2. Chemical Reduction

Compound **3c** (2.14 mg, 5.9 μ mol), nitrogen purged acetonitrile, ammonium chloride, and zinc powder were transferred to a Pd/C catalyzed anaerobic chamber with an atmosphere of 5% H₂, 5% CO₂, 90% N₂ (Shellab Bacatron, Sheldon Manufacturing Inc. Cornelius, OR). **3c** was dissolved in acetonitrile (1 mL), followed by addition of NH₄Cl (32.1 mg, 0.60 mmol) and zinc powder (32.6 mg, 0.50 mmol). The resulting slurry was mixed and left for 1 h, then filtered through 0.2 μ m acrodisc filters. Filtrate samples were diluted in mobile phase (1:100) and analyzed immediately by LC/MS, or after 3 h incubation at room temperature.

3.2.3. LC/MS Analysis

Solutions were analyzed with an Agilent 1260 series HPLC coupled with an Agilent single stage quadrupole mass spectrometer, equipped with a Jet StreamTM electrospray ionization source (Agilent Technologies, USA). Chromatographic separation was achieved on an Agilent Zorbax C18, 3.0 × 150 mm column with 5 μ m particle size, maintained at 30 °C. The mobile phase consisted of 45 mM ammonium formate buffer, pH 3.5 (A) and 80% acetonitrile with 0.01% formic acid (B) with a linear gradients (40–100% B over 8 min, 100–40% B over 1 min, held at 40% B for 3 min) at a flow rate of 0.5 mL/min. The sample volume injected was 100 μ L and the auto sampler was set at 4 °C. The mass spectrometer was run in positive and negative ion ionization modes, with dual polarity scans from 100–600 m/z . Instrument parameters of the mass spectrometer were: fragmentation voltage 70 V, gas flow 12 L/min, gas temperature 250 °C, sheath gas flow 10 L/min, sheath gas temperature 325 °C, nebuliser 35 psi, capillary voltage 2500 V, and nozzle voltage 500V. Absorbance detection was at 276 nm (bandwidth 16 nm) with quantitation by integration of peak areas with Agilent Open Lab CDS Chemstation software. Unirradiated samples were used for single-point calibration.

3.2.4. Biochemical PARP Inhibition Assay

Inhibition of PARP-1 activity was evaluated in a radioisotope-based filter binding assay by Reaction Biology Corporation (Malvern PA) using human recombinant PARP-1 (residues 1-1014, Genbank accession # NM_001618.3, MW = 114.8 kDa) expressed with a C-terminal His-tag in Sf9 insect cells, >80% pure by SDS-PAGE. Polymerization of ³²P-NAD⁺ (10 μ M) on core histones (0.01 mg/mL) in buffer (50 mM Tris-HCl, 50 mM NaCl, 10 mM MgCl₂, 0.02% Brij35, 1 mM DTT, 1% DMSO and 20 μ g/mL activated DNA (Sigma-Aldrich D4522) was measured after 1 h incubation and washout of remaining free NAD⁺. Each compound was included in a 10-point, 3-fold dilution dose response experiment and an IC₅₀ value derived.

Author Contributions: Conceptualization, M.P.H. and W.R.W.; investigation, B.D.D. and W.-W.W.; resources, M.P.H. and W.R.W.; writing—original draft preparation, B.D.D.; visualization, W.-W.W.; writing—review and editing, B.D.D., M.P.H. and W.R.W.; supervision, M.P.H. and W.R.W.; funding acquisition, M.P.H. and W.R.W.

Funding: This research was funded by the Health Research Council of New Zealand grant number 14/538 and the Cancer Research Trust New Zealand grant numbers GOT-1606 and GOT-1349.

Acknowledgments: The authors thank Adrian Blaser for assistance with NMR spectroscopy and Sisira Kumara for HPLC analyses.

Conflicts of Interest: The authors declare no conflict of interest. The funders had no role in the design of the study; in the collection, analyses, or interpretation of data; in the writing of the manuscript; and in the decision to publish the results.

Abbreviations

- AcCl acetyl chloride;
- BnCl benzyl chloride;
- CDI 1,1'-carbonyldiimidazole;
- DCM dichloromethane;
- DIPEA diisopropylethylamine;
- DMF *N,N*-dimethylformamide;
- EtOAc ethyl acetate;
- Et₂O diethyl ether;
- EtOH ethanol;
- h hour;
- MeOH methanol;
- rt room temperature;
- THF tetrahydrofuran;
- X4 petroleum ether boiling range 40–60 °C.

References

1. De Lorenzo, S.B.; Patel, A.G.; Hurley, R.M.; Kaufmann, S.H. The Elephant and the Blind Men: Making Sense of PARP Inhibitors in Homologous Recombination Deficient Tumor Cells. *Front. Oncol.* **2013**, *3*, 228. [[CrossRef](#)] [[PubMed](#)]
2. Durkacz, B.W.; Omidiji, O.; Gray, D.A.; Shall, S. (ADP-ribose)_n participates in DNA excision repair. *Nature* **1980**, *283*, 593–596. [[CrossRef](#)]
3. Sousa, F.G.; Matuo, R.; Soares, D.G.; Escargueil, A.E.; Henriques, J.A.P.; Larsen, A.K.; Saffi, J. PARPs and the DNA damage response. *Carcinogenesis* **2012**, *33*, 1433–1440. [[CrossRef](#)] [[PubMed](#)]
4. Krishnakumar, R.; Kraus, W.L. The PARP Side of the Nucleus: Molecular Actions, Physiological Outcomes, and Clinical Targets. *Mol. Cell* **2010**, *39*, 8–24. [[CrossRef](#)] [[PubMed](#)]
5. Satoh, M.S.; Lindahl, T. Role of poly(ADP-ribose) formation in DNA repair. *Nature* **1992**, *356*, 356–358. [[CrossRef](#)]
6. Helleday, T. The underlying mechanism for the PARP and BRCA synthetic lethality: Clearing up the misunderstandings. *Mol. Oncol.* **2011**, *5*, 387–393. [[CrossRef](#)] [[PubMed](#)]
7. Dantzer, F.; Schreiber, V.; Niedergang, C.; Trucco, C.; Flatter, E.; Rubia, G.D.L.; Oliver, J.; Rolli, V.; Ménissier-de Murcia, J.; de Murcia, G. Involvement of poly(ADP-ribose) polymerase in base excision repair. *Biochimie* **1999**, *81*, 69–75. [[CrossRef](#)]
8. Ström, C.E.; Johansson, F.; Uhlén, M.; Szigyarto, C.A.-K.; Erixon, K.; Helleday, T. Poly (ADP-ribose) polymerase (PARP) is not involved in base excision repair but PARP inhibition traps a single-strand intermediate. *Nucleic Acids Res.* **2011**, *39*, 3166–3175. [[CrossRef](#)]
9. Murai, J.; Huang, S.N.; Das, B.B.; Renaud, A.; Zhang, Y.; Doroshov, J.H.; Ji, J.; Takeda, S.; Pommier, Y. Trapping of PARP1 and PARP2 by Clinical PARP Inhibitors. *Cancer Res.* **2012**, *72*, 5588–5599. [[CrossRef](#)]
10. Murai, J.; Huang, S.-Y.N.; Renaud, A.; Zhang, Y.; Ji, J.; Takeda, S.; Morris, J.; Teicher, B.; Doroshov, J.H.; Pommier, Y. Stereospecific PARP Trapping by BMN 673 and Comparison with Olaparib and Rucaparib. *Mol. Cancer Ther.* **2014**, *13*, 433–443. [[CrossRef](#)] [[PubMed](#)]
11. Shen, Y.; Aoyagi-Scharber, M.; Wang, B. Trapping Poly(ADP-Ribose) Polymerase. *J. Pharmacol. Exp. Ther.* **2015**, *353*, 446–457. [[CrossRef](#)] [[PubMed](#)]

12. Bryant, H.E.; Schultz, N.; Thomas, H.D.; Parker, K.M.; Flower, D.; Lopez, E.; Kyle, S.; Meuth, M.; Curtin, N.J.; Helleday, T. Specific killing of BRCA2-deficient tumours with inhibitors of poly(ADP-ribose) polymerase. *Nature* **2005**, *434*, 913–917. [[CrossRef](#)] [[PubMed](#)]
13. Farmer, H.; McCabe, N.; Lord, C.J.; Tutt, A.N.J.; Johnson, D.A.; Richardson, T.B.; Santarosa, M.; Dillon, K.J.; Hickson, I.; Knights, C.; et al. Targeting the DNA repair defect in BRCA mutant cells as a therapeutic strategy. *Nature* **2005**, *434*, 917–921. [[CrossRef](#)] [[PubMed](#)]
14. Lord, C.J.; Ashworth, A. PARP inhibitors: Synthetic lethality in the clinic. *Science* **2017**, *355*, 1152–1158. [[CrossRef](#)]
15. Nirsimloo, R.; Gourley, C. The safety and efficacy of olaparib therapy in patients with relapsed ovarian cancer. *Expert Rev. Anticancer Ther.* **2016**, *16*, 597–603. [[CrossRef](#)]
16. Curtin, N.J.; Szabo, C. Therapeutic applications of PARP inhibitors: Anticancer therapy and beyond. *Mol. Aspects Med.* **2013**, *34*, 1217–1256. [[CrossRef](#)]
17. Ali, S.O.; Khan, F.A.; Galindo-Campos, M.A.; Yélamos, J. Understanding specific functions of PARP-2: New lessons for cancer therapy. *Am. J. Cancer Res.* **2016**, *6*, 1842–1863.
18. Sallmyr, A.; Tomkinson, A.E. Repair of DNA double-strand breaks by mammalian alternative end-joining pathways. *J. Biol. Chem.* **2018**, *293*, 10536–10546. [[CrossRef](#)]
19. Chalmers, A.J.; Lakshman, M.; Chan, N.; Bristow, R.G. Poly(ADP-Ribose) Polymerase Inhibition as a Model for Synthetic Lethality in Developing Radiation Oncology Targets. *Semin. Radiat. Oncol.* **2010**, *20*, 274–281. [[CrossRef](#)]
20. Veuger, S.J.; Curtin, N.J.; Richardson, C.J.; Smith, G.C.M.; Durkacz, B.W. Radiosensitization and DNA Repair Inhibition by the Combined Use of Novel Inhibitors of DNA-dependent Protein Kinase and Poly(ADP-Ribose) Polymerase-1. *Cancer Res.* **2003**, *63*, 6008–6015.
21. Dréan, A.; Lord, C.J.; Ashworth, A. PARP inhibitor combination therapy. *Crit. Rev. Oncol. Hematol.* **2016**, *108*, 73–85. [[CrossRef](#)] [[PubMed](#)]
22. Oza, A.M.; Cibula, D.; Benzaquen, A.O.; Poole, C.; Mathijssen, R.H.J.; Sonke, G.S.; Colombo, N.; Špaček, J.; Vuylsteke, P.; Hirte, H.; et al. Olaparib combined with chemotherapy for recurrent platinum-sensitive ovarian cancer: A randomised phase 2 trial. *Lancet Oncol.* **2015**, *16*, 87–97. [[CrossRef](#)]
23. Rajan, A.; Carter, C.A.; Kelly, R.J.; Gutierrez, M.; Kummar, S.; Szabo, E.; Yancey, M.A.; Ji, J.; Mannargudi, B.; Woo, S.; et al. A Phase I Combination Study of Olaparib with Cisplatin and Gemcitabine in Adults with Solid Tumors. *Clin. Cancer Res.* **2012**, *18*, 2344–2351. [[CrossRef](#)] [[PubMed](#)]
24. Kummar, S.; Chen, A.; Ji, J.; Zhang, Y.; Reid, J.M.; Ames, M.; Jia, L.; Weil, M.; Speranza, G.; Murgo, A.J.; et al. Phase I Study of PARP Inhibitor ABT-888 in Combination with Topotecan in Adults with Refractory Solid Tumors and Lymphomas. *Cancer Res.* **2011**, *71*, 5626–5634. [[CrossRef](#)] [[PubMed](#)]
25. Liu, J.F.; Barry, W.T.; Birrer, M.; Lee, J.-M.; Buckanovich, R.J.; Fleming, G.F.; Rimel, B.; Buss, M.K.; Nattam, S.; Hurteau, J.; et al. Combination cediranib and olaparib versus olaparib alone for women with recurrent platinum-sensitive ovarian cancer: A randomised phase 2 study. *Lancet Oncol.* **2014**, *15*, 1207–1214. [[CrossRef](#)]
26. Plummer, R.; Jones, C.; Middleton, M.; Wilson, R.; Evans, J.; Olsen, A.; Curtin, N.; Boddy, A.; McHugh, P.; Newell, D.; et al. Phase I Study of the Poly(ADP-Ribose) Polymerase Inhibitor, AG014699, in Combination with Temozolomide in Patients with Advanced Solid Tumors. *Clin. Cancer Res.* **2008**, *14*, 7917–7923. [[CrossRef](#)]
27. Plummer, R.; Stephens, P.; Aissat-Daudigny, L.; Cambois, A.; Moachon, G.; Brown, P.D.; Campone, M. Phase 1 dose-escalation study of the PARP inhibitor CEP-9722 as monotherapy or in combination with temozolomide in patients with solid tumors. *Cancer Chemother. Pharmacol.* **2014**, *74*, 257–265. [[CrossRef](#)] [[PubMed](#)]
28. Samol, J.; Ranson, M.; Scott, E.; Macpherson, E.; Carmichael, J.; Thomas, A.; Cassidy, J. Safety and tolerability of the poly(ADP-ribose) polymerase (PARP) inhibitor, olaparib (AZD2281) in combination with topotecan for the treatment of patients with advanced solid tumors: A phase I study. *Investig. New Drugs* **2012**, *30*, 1493–1500. [[CrossRef](#)]
29. Wilson, W.R.; Hay, M.P. Targeting hypoxia in cancer therapy. *Nat. Rev. Cancer* **2011**, *11*, 393–410. [[CrossRef](#)]
30. Vaupel, P.; Mayer, A. Hypoxia in cancer: Significance and impact on clinical outcome. *Cancer Metastasis Rev.* **2007**, *26*, 225–239. [[CrossRef](#)]
31. Harris, A.L. Hypoxia—A key regulatory factor in tumour growth. *Nat. Rev. Cancer* **2002**, *2*, 38–47. [[CrossRef](#)]
32. Phillips, R.M. Targeting the hypoxic fraction of tumours using hypoxia-activated prodrugs. *Cancer Chemother. Pharmacol.* **2016**, *77*, 441–457. [[CrossRef](#)]

33. Brown, J.M.; Wilson, W.R. Exploiting tumour hypoxia in cancer treatment. *Nat. Rev. Cancer* **2004**, *4*, 437–447. [[CrossRef](#)]
34. Horsman, M.R.; Vaupel, P. Pathophysiological Basis for the Formation of the Tumor Microenvironment. *Front. Oncol.* **2016**, *6*, 66. [[CrossRef](#)]
35. O'Connor, L.J.; Cazares-Körner, C.; Saha, J.; Evans, C.N.G.; Stratford, M.R.L.; Hammond, E.M.; Conway, S.J. Design, synthesis and evaluation of molecularly targeted hypoxia-activated prodrugs. *Nat. Protoc.* **2016**, *11*, 781–794. [[CrossRef](#)] [[PubMed](#)]
36. Hong, C.R.; Dickson, B.D.; Jaiswal, J.K.; Pruijn, F.B.; Hunter, F.W.; Hay, M.P.; Hicks, K.O.; Wilson, W.R. Cellular pharmacology of evofosfamide (TH-302): A critical re-evaluation of its bystander effects. *Biochem. Pharmacol.* **2018**, *156*, 265–280. [[CrossRef](#)]
37. Meng, F.; Evans, J.W.; Bhupathi, D.; Banica, M.; Lan, L.; Lorente, G.; Duan, J.-X.; Cai, X.; Mowday, A.M.; Guise, C.P.; et al. Molecular and Cellular Pharmacology of the Hypoxia-Activated Prodrug TH-302. *Mol. Cancer Ther.* **2011**, *11*, 740–751. [[CrossRef](#)] [[PubMed](#)]
38. Patterson, A.V.; Ferry, D.M.; Edmunds, S.J.; Gu, Y.; Singleton, R.S.; Patel, K.; Pullen, S.M.; Hicks, K.O.; Syddall, S.P.; Atwell, G.J.; et al. Mechanism of Action and Preclinical Antitumor Activity of the Novel Hypoxia-Activated DNA Cross-Linking Agent PR-104. *Clin. Cancer Res.* **2007**, *13*, 3922–3932. [[CrossRef](#)] [[PubMed](#)]
39. Menear, K.A.; Adcock, C.; Boulter, R.; Cockcroft, X.; Copsey, L.; Cranston, A.; Dillon, K.J.; Drzewiecki, J.; Garman, S.; Gomez, S.; et al. 4-[3-(4-Cyclopropanecarbonylpiperazine-1-carbonyl)-4-fluorobenzyl]-2H-phthalazin-1-one: A Novel Bioavailable Inhibitor of Poly(ADP-ribose) Polymerase-1. *J. Med. Chem.* **2008**, *51*, 6581–6591. [[CrossRef](#)] [[PubMed](#)]
40. Ferraris, D.V. Evolution of Poly(ADP-ribose) Polymerase-1 (PARP-1) Inhibitors. From Concept to Clinic. *J. Med. Chem.* **2010**, *53*, 4561–4584. [[CrossRef](#)]
41. Thorsell, A.-G.; Ekblad, T.; Karlberg, T.; Löw, M.; Pinto, A.F.; Trésaugues, L.; Moche, M.; Cohen, M.S.; Schüler, H. Structural Basis for Potency and Promiscuity in Poly(ADP-ribose) Polymerase (PARP) and Tankyrase Inhibitors. *J. Med. Chem.* **2017**, *60*, 1262–1271. [[CrossRef](#)] [[PubMed](#)]
42. Berry, J.M.; Watson, C.Y.; Whish, W.J.D.; Threadgill, M.D. 5-Nitrofuranyl-methyl group as a potential bioreductively activated pro-drug system. *J. Chem. Soc. Perkin Trans. 1* **1997**, 1147–1156. [[CrossRef](#)]
43. Parveen, I.; Naughton, D.P.; Whish, W.J.D.; Threadgill, M.D. 2-Nitroimidazol-5-ylmethyl as a potential bioreductively activated prodrug system: Reductively triggered release of the parp inhibitor 5-bromoisoquinolinone. *Bioorg. Med. Chem. Lett.* **1999**, *9*, 2031–2036. [[CrossRef](#)]
44. Lindquist, K.E.; Cran, J.D.; Kordic, K.; Chua, P.C.; Winters, G.C.; Tan, J.S.; Lozada, J.; Kyle, A.H.; Evans, J.W.; Minchinton, A.I. Selective radiosensitization of hypoxic cells using BCCA621C: A novel hypoxia activated prodrug targeting DNA-dependent protein kinase. *Tumor Microenviron. Ther.* **2013**, *1*, 46–55. [[CrossRef](#)]
45. Thomson, P.; Naylor, M.A.; Everett, S.A.; Stratford, M.R.L.; Lewis, G.; Hill, S.; Patel, K.B.; Wardman, P.; Davis, P.D. Synthesis and biological properties of bioreductively targeted nitrothienyl prodrugs of combretastatin A-4. *Mol. Cancer Ther.* **2006**, *5*, 2886–2894. [[CrossRef](#)]
46. Lin, C.-F.; Yang, J.-S.; Chang, C.-Y.; Kuo, S.-C.; Lee, M.-R.; Huang, L.-J. Synthesis and anticancer activity of benzyloxybenzaldehyde derivatives against HL-60 cells. *Bioorg. Med. Chem.* **2005**, *13*, 1537–1544. [[CrossRef](#)] [[PubMed](#)]
47. Griffin, R.J.; Srinivasan, S.; Bowman, K.; Calvert, A.H.; Curtin, N.J.; Newell, D.R.; Pemberton, L.C.; Golding, B.T. Resistance-Modifying Agents. 5. Synthesis and Biological Properties of Quinazolinone Inhibitors of the DNA Repair Enzyme Poly(ADP-ribose) Polymerase (PARP). *J. Med. Chem.* **1998**, *41*, 5247–5256. [[CrossRef](#)]
48. Matteucci, M.; Duan, J.-X.; Jiao, H.; Kaizerman, J.; Ammons, S. Phosphoramidate Alkylator Prodrugs. U.S. Patent US 8,003,625, 23 August 2011.
49. Winn, B.A.; Shi, Z.; Carlson, G.J.; Wang, Y.; Nguyen, B.L.; Kelly, E.M.; Ross, R.D.; Hamel, E.; Chaplin, D.J.; Trawick, M.L.; et al. Bioreductively activatable prodrug conjugates of phenstatin designed to target tumor hypoxia. *Bioorg. Med. Chem. Lett.* **2017**, *27*, 636–641. [[CrossRef](#)] [[PubMed](#)]
50. Ferrer, S.; Naughton, D.P.; Parveen, I.; Threadgill, M.D. N- and O-Alkylation of isoquinolin-1-ones in the Mitsunobu reaction: Development of potential drug delivery systems. *J. Chem. Soc. Perkin Trans. 1* **2002**, *3*, 335–340. [[CrossRef](#)]

51. Buxton, G.V. *Radiation Chemistry of the Liquid State*; VCH Publishers Inc.: New York, NY, USA, 1987; ISBN 0-89573-127-4.
52. Mulazzani, Q.G.; D'Angelantonio, M.; Venturi, M.; Hoffman, M.Z.; Rodgers, M.A.J. Interaction of formate and oxalate ions with radiation-generated radicals in aqueous solution. Methylviologen as a mechanistic probe. *J. Phys. Chem.* **1986**, *90*, 5347–5352. [[CrossRef](#)]
53. Hay, M.P.; Wilson, W.R.; Denny, W.A. Design, Synthesis and Evaluation of Imidazolylmethyl Carbamate Prodrugs of Alkylating Agents. *Tetrahedron* **2000**, *56*, 645–657. [[CrossRef](#)]
54. Sykes, B.M.; Hay, M.P.; Bohinc-Herceg, D.; Helsby, N.A.; O'Connor, C.J.; Denny, W.A. Leaving group effects in reductively triggered fragmentation of 4-nitrobenzyl carbamates. *J. Chem. Soc. Perkin Trans. 1* **2000**, *10*, 1601–1608. [[CrossRef](#)]
55. Everett, S.A.; Naylor, M.A.; Patel, K.B.; Stratford, M.R.L.; Wardman, P. Bioreductively-activated prodrugs for targeting hypoxic tissues: Elimination of aspirin from 2-nitroimidazole derivatives. *Bioorg. Med. Chem. Lett.* **1999**, *9*, 1267–1272. [[CrossRef](#)]
56. Duan, J.-X.; Jiao, H.; Kaizerman, J.; Stanton, T.; Evans, J.W.; Lan, L.; Lorente, G.; Banica, M.; Jung, D.; Wang, J.; et al. Potent and Highly Selective Hypoxia-Activated Achiral Phosphoramidate Mustards as Anticancer Drugs. *J. Med. Chem.* **2008**, *51*, 2412–2420. [[CrossRef](#)] [[PubMed](#)]
57. Munín, J.; Santana, L.; Uriarte, E.; Borges, F.; Quezada, E. A comparative synthesis of 6-benzyl-2,3-dihydroimidazo[2,1-a]phthalazine and 2H-7-benzyl-3,4-dihydropyrimido[2,1-a]phthalazine. *Tetrahedron Lett.* **2015**, *56*, 828–830. [[CrossRef](#)]
58. Bouider, N.; Fhayli, W.; Ghandour, Z.; Boyer, M.; Harrouche, K.; Florence, X.; Pirotte, B.; Lebrun, P.; Faury, G.; Khelili, S. Design and synthesis of new potassium channel activators derived from the ring opening of diazoxide: Study of their vasodilatory effect, stimulation of elastin synthesis and inhibitory effect on insulin release. *Bioorg. Med. Chem.* **2015**, *23*, 1735–1746. [[CrossRef](#)] [[PubMed](#)]
59. Su, J.; Chen, Q.; Lu, L.; Ma, Y.; Auyoung, G.H.L.; Hua, R. Base-promoted nucleophilic fluoroarenes substitution of CF bonds. *Tetrahedron* **2018**, *74*, 303–307. [[CrossRef](#)]
60. Ghosh, S.K.; Nagarajan, R. Total synthesis of penipanoid C, 2-(4-hydroxybenzyl)quinazolin-4(3H)-one and NU1025. *Tetrahedron Lett.* **2016**, *57*, 4277–4279. [[CrossRef](#)]
61. Abe, Y.; Kayakiri, H.; Satoh, S.; Inoue, T.; Sawada, Y.; Inamura, N.; Asano, M.; Aramori, I.; Hatori, C.; Sawai, H.; et al. A Novel Class of Orally Active Non-Peptide Bradykinin B2 Receptor Antagonists. 3. Discovering Bioisosteres of the Imidazo[1,2-a]pyridine Moiety. *J. Med. Chem.* **1998**, *41*, 4062–4079. [[CrossRef](#)]
62. Cavalleri, B.; Ballotta, R.; Arioli, V.; Lancini, G. New 5-substituted 1-alkyl-2-nitroimidazoles. *J. Med. Chem.* **1973**, *16*, 557–560. [[CrossRef](#)] [[PubMed](#)]
63. Dalton, N.; Gordon, C.P.; Boyle, T.P.; Vandegraaf, N.; Deadman, J.; Rhodes, D.I.; Coates, J.A.; Pyne, S.G.; Keller, P.A.; Bremner, J.B. The discovery of allyltyrosine based tripeptides as selective inhibitors of the HIV-1 integrase strand-transfer reaction. *Org. Biomol. Chem.* **2016**, *14*, 6010–6023. [[CrossRef](#)] [[PubMed](#)]
64. Cheng, J.M.H.; Liu, L.; Pellicci, D.G.; Reddiex, S.J.J.; Cotton, R.N.; Cheng, T.-Y.; Young, D.C.; Van Rhijn, I.; Moody, D.B.; Rossjohn, J.; et al. Total Synthesis of Mycobacterium tuberculosis Dideoxymycobactin-838 and Stereoisomers: Diverse CD1a-Restricted T Cells Display a Common Hierarchy of Lipopeptide Recognition. *Chem. Eur. J.* **2017**, *23*, 1694–1701. [[CrossRef](#)] [[PubMed](#)]
65. Fricke, J.; Hart, E.J. Chemical Dosimetry. In *Radiation Dosimetry vol 2*; Attix, F.H., Roesch, W.C., Eds.; Academic Press: New York, NY, USA, 1966; pp. 167–239.

Sample Availability: Samples of the compounds 4–13 are available from the authors.



© 2019 by the authors. Licensee MDPI, Basel, Switzerland. This article is an open access article distributed under the terms and conditions of the Creative Commons Attribution (CC BY) license (<http://creativecommons.org/licenses/by/4.0/>).